Plasma-catalytic ammonia reforming of methane over Cu-based catalysts for the production of HCN and H2 at reduced temperature

Plasma-catalytic Ammonia Reforming of Methane over Cu-based Catalysts for the Production of HCN and H_2 at Reduced Temperature

Yanhui Yi,*[,1,2,#] Xin Wang,[1,#] Amin Jafarzadeh,[2,#] Li Wang,[3] Pei Liu,[4] Bowen He,[4] Jinhui Yan,[1] Rui Zhang,[1] Hantian Zhang,[2] Xi Liu,[4] Hongchen Guo,[1] Erik C. Neyts,[2] and Annemie Bogaerts[2]

[1]State Key Laboratory of Fine Chemicals, School of Chemical Engineering, Dalian University of Technology, Dalian 116024, P.R. China.

[2]Research group PLASMANT, Department of Chemistry, University of Antwerp, Universiteitsplein 1, BE-2610 Wilrijk-Antwerp, Belgium Department

[3]College of Environmental Sciences and Engineering, Dalian Maritime University, Dalian 116026, Liaoning, P. R. China.

[4]In-situ Center for Physical Sciences, School of Chemistry and Chemical Engineering, Shanghai Jiao Tong University, Shanghai 200240, P.R. China

#: these authors contributed equally (shared first authors)

ABSTRACT: Industrial production of HCN from NH_3 and CH_4 not only uses precious Pt or Pt-Rh catalysts, but also requires extremely high temperatures (~1,600 K). From an energetic, operational and safety perspective, a drastic decrease in temperature is highly desirable. Here we report ammonia reforming of methane (ARM) for the production of HCN and H_2 at 673 K by the combination of CH_4/NH_3 plasma and a supported Cu/Silicalite-1 catalyst. 30 % CH_4 conversion has been achieved with 79 % HCN selectivity. Catalyst characterization and plasma diagnostics reveal that the excellent reaction performance is attributed to metallic Cu active sites. In addition, we propose a possible reaction pathway, viz. E-R reactions with N, NH, NH_2 and CH radicals produced in the plasma, for the production of HCN, based on DFT calculations. Importantly, the Cu/Silicalite-1 catalyst costs less than 5% of the commercial Pt mesh catalyst.

KEYWORDS: *ammonia reforming of methane, plasma catalysis, C-N coupling reaction, HCN synthesis, hydrogen production*

INTRODUCTION

Hydrocyanic acid (HCN), an important organic chemical featured by the C≡N functional group, is widely used in medicine, metallurgy, for pesticides, fuels and polymers.[1,2] Driven by the demand for plastics and polymers, such as nylon and plexiglass in the 1950s, BASF corporation created the first facility for industrial production of HCN. The annual production of HCN in 1956 was only 2,400 tons, but it has increased to more than 100,000 tons/year today,[1] which is mainly achieved by the Andrussow process or the BMA process.

The Andrussow process is an exothermic reaction of CH_4, NH_3 and O_2 (equation (1)). It is usually realized over a Pt-Rh alloy gauze catalyst at atmospheric pressure and 1,300-1,400 K. The required energy to maintain the high temperature is mainly supplied by combustion of H_2, which leads to a waste of H_2 energy. Alloying of Pt by Rh (10 % Rh) to form a Pt-Rh alloy gauze catalyst is necessary to improve the durability of the catalyst, because of the high reaction temperature, which usually results in inactivation of Pt. In addition, the high temperature also results in a long time for feed gas heating and product cooling. Generally, about 60 % HCN yield and 60-70 % NH_3 utilization can be achieved by the Andrussow process.[1-4]

$$CH_4 + NH_3 + 1.5O_2 \rightarrow HCN + 3H_2O \quad \triangle H^0_{298K} = -483 \text{ kJ/mol} \quad (1)$$

In contrast, the Blausaure Methane Anlage (BMA) process is a strongly endothermic reaction between CH_4 and NH_3 (equation (2)). It is usually operated at atmospheric pressure for HCN synthesis with stoichiometric hydrogen production, which is a significant advantage compared to the Andrussow process.

$$CH_4 + NH_3 \rightarrow HCN + 3H_2 \quad \triangle H^0_{298K} = 251 \text{ kJ/mol} \quad (2)$$

This BMA process is also called Degussa process, as it was firstly exploited by Degussa company in Wesseling.[3,4] In industrial BMA plants, the Pt mesh catalyst is usually placed in parallel columnar reactors. The equilibrium conversion, selectivity and yield as a function of temperature, obtained through thermodynamic calculation, are plotted in Figure S1. The BMA process for HCN synthesis is typically operated at a temperature of ~1,600 K, to balance the HCN yield and cost. On the one hand, the HCN yield increases with reaction temperature; on the other hand, the high reaction temperature also causes a higher investment of equipment, as well as energy consumption and waste of feed gas; indeed, a great amount of NH_3 and CH_4 is decomposed into N_2 and coke, respectively.[1-4]

Although the Andrussow process and the BMA process have been used in industrial HCN production for many decades, research is still being conducted on optimizing the reaction conditions[5,6] and uncovering the mechanism of C-N coupling over Pt and Pt-Rh catalysts.[7-11] To our knowledge, there are currently no methods available to synthesize HCN at temperatures below 1,300-1,400 K for the Andrussow process, and below 1,600 K for the BMA process.

The non-equilibrium character of non-thermal plasma (NTP), i.e., ionized gas, consisting of molecules, but also electrons, ions, radicals and excited species, offers a unique approach to enable some thermodynamically unfavorable chemical reactions at low temperature.[12-14] The gas temperature in such plasma can be maintained even as low as room temperature. The generated electrons, however, are highly energetic with a typical energy of 1-10 eV, or 10^4-10^5 K. Therefore, these energetic electrons can activate reactant molecules (e.g., CH_4 and NH_3) into reactive species, i.e., radicals, excited atoms and molecules, and ions, which can easily trigger chemical reactions at room temperature.

Inspired by the catalytic activity of Pt in HCN synthesis (both in the Andrussow process and BMA process), we previously combined supported Pt catalysts with CH_4/NH_3 NTP for HCN synthesis, in so-called plasma catalysis.[15] HCN was produced from a CH_4/NH_3 mixture at 673 K, reaching 26 % CH_4 conversion and 81 % HCN selectivity when using optimized catalysts, i.e., Pt/TS-1 catalyst (Pt supported on Titanium silicalite-1 zeolite). However, this Pt/TS-1 catalyst is extremely expensive, because of the high price of Pt caused by scarcity, and the high price of the TS-1 support caused by the long and multistep synthesis process, the expensive titanium precursor (tetraethyl titanate) and organic amine template (tetrapropylammonium hydroxide). Therefore, it is crucial to examine possible lower cost catalysts by only using non-noble metals and low-cost supports, for practical application of plasma-catalytic HCN synthesis.

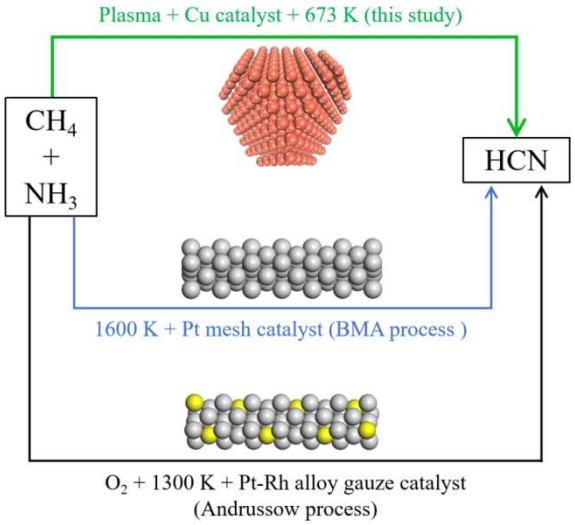

Figure 1. Schematic diagram of the classical methods for HCN synthesis, and our novel method, presented in this paper.

In this paper, we report ammonia reforming of methane (ARM) for co-production of HCN and H_2 at 673 K by the combination of CH_4/NH_3 NTP and a Cu/Silicalite-1 (Cu/S-1) catalyst (Figure 1), reaching 30 % CH_4 conversion with 79 % HCN selectivity. The novelty of this work compared to our previous paper is (i) the use of a lower cost Cu catalyst to replace expensive Pt, (ii) the use of lower cost Silicalite-1 zeolite (S-1) support to replace expensive Titanium Silicalite-1 zeolite support, and (iii) DFT calculations to explain the E-R reaction mechanism in plasma catalysis. In general, using lower cost catalysts and milder conditions to realize important reactions for chemical production is one of the major goals in catalysis research. Interestingly, we reduced the cost of the catalyst (Cu/S-1) by 95 % compared to the commercial Pt mesh catalyst, and by 80 % compared to the Pt/TS-1 catalyst. Furthermore, stoichiometric H_2 is produced as well, which can be separated from the mixture and used as green energy. The experimental details are presented in the supporting information.

RESULTS and DISCUSSION

Figure 2 presents the catalytic performance of the Cu/S-1 catalyst in the ARM reaction. In the absence of plasma, i.e., only using the Cu/S-1 catalyst, the CH_4 conversion is zero, demonstrating that the ARM reaction cannot be triggered at 673 K without the help of plasma. When using a CH_4/NH_3 plasma (673 K), but not using any catalyst, the conversion reaches 11.1 %. When we pack the CH_4/NH_3 plasma by S-1 granules, the CH_4 conversion rises to 15.6 % (673 K), and it further increases to 30 % when using the Cu/S-1 catalyst.

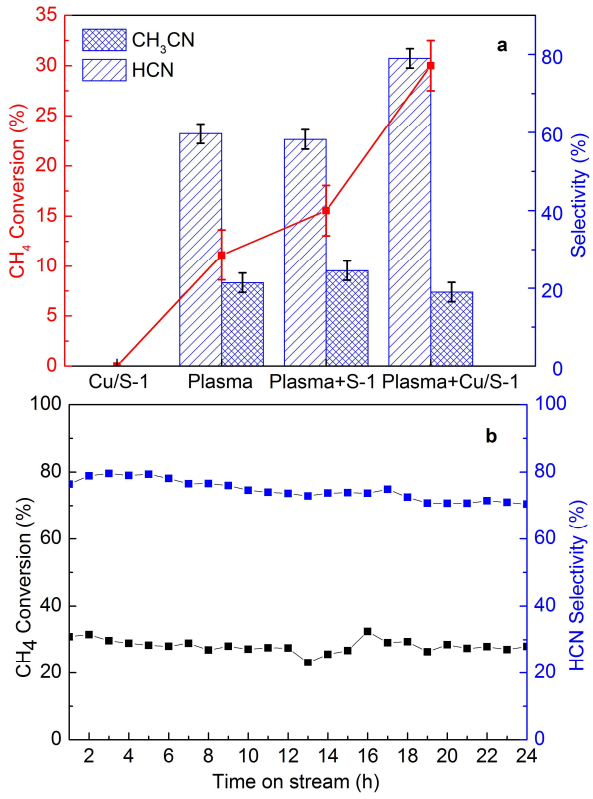

Figure 2. CH_4 conversion and selectivity towards HCN and CH_3CN at 673 K, for (a) catalyst only, plasma only, plasma + S-1 support, and plasma + Cu/S-1 catalyst, and (b) for 24 h, to test the stability of Cu/S-1 catalyst (Reaction condition: 10 wt.% Cu loading, CH_4 : NH_3 = 1 : 2, GHSV: 1529 h^{-1}, discharge length: 5 cm, the error bars are obtained from five repetitions of the experiment).

In terms of HCN selectivity, there is little difference between "plasma" and "plasma + S-1", i.e., around 60 %, while the HCN selectivity rises to 79 % in case of "plasma + Cu/S-1". In addition to HCN, the main byproduct was qualitatively analyzed as acetonitrile (CH_3CN); see Figure S2. Furthermore, some other more complex compounds, i.e., N, N-dimethyl

cyanamide [$(CH_3)_2NCN$)] and amino acetonitrile (NH_2CH_2CN), were detected as well. The selectivity results shown in Figure 2 were obtained through the C-balance of the total amount of products. Interestingly, no C_2 or larger hydrocarbons were detected by GC (Figure S3), indicating that virtually no C−C coupling to hydrocarbons occurred. The H_2 content in the product was found to be consistent with the stoichiometry of reaction (2). In addition, little N_2 was detected (Figure S3), illustrating that NH_3 was hardly decomposed into N_2, attributed to the poor activity of Cu catalysts towards NH_3 decomposition. The above results indicate that plasma catalysis, i.e., the combination of CH_4/NH_3 plasma and Cu/S-1 catalyst, can dramatically improve both CH_4 conversion and HCN selectivity compared to only Cu/S-1 catalyst or only CH_4/NH_3 plasma. This result implies the possibility to efficiently realize the ARM reaction at low temperature for the production of HCN, CH_3CN and H_2, without C_2 or larger hydrocarbons or N_2.

The energy efficiency for the synthesis of HCN and CH_3CN in the plasma-catalytic ARM reaction is 6.0 %, which is much higher than that of plasma only (1.8 %) and that of plasma + S-1 (2.3 %), as shown in Figure S4. The energy consumption for producing HCN in the plasma-catalytic ARM reaction is 5.2 kJ/mmol, which is much lower than that of plasma only (18.1 kJ/mmol) and that of plasma + S-1 (14.5 kJ/mmol), showing the key role of Cu-based catalyst in improving the reaction performance.

Although the energy consumption in this paper (5.2 kJ/mmol) is higher than the BMA process (1.1 kJ/mmol),[16] the use of Cu-based catalyst instead of Pt-based catalyst should also be considered when looking at the overall cost, and the lower temperature allowing safer operation conditions is an important advantage. The discharge power, needed to calculate the energy efficiency, was obtained by the waveforms of discharge voltage and discharge current (Figure S5).

We also studied the effects of reaction temperature and Cu loading on the CH_4 conversion and HCN selectivity, as shown in Figure S6. Our measurements indicate that a relatively high temperature is favorable for the ARM reaction to produce HCN, while higher loadings (15 %-30 %) can slightly further improve the CH_4 conversion and HCN selectivity. In the case of 30 wt.% Cu loading, we achieved 32.4 % CH_4 conversion

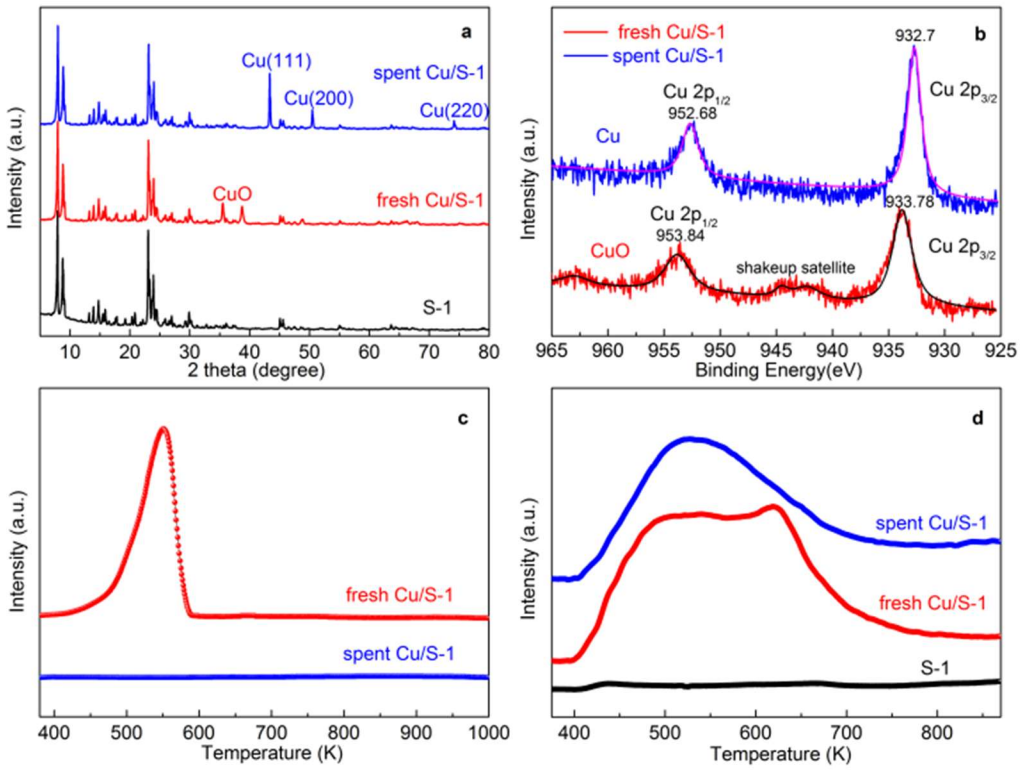

Figure 3. Characterization results of the fresh and spent Cu/S-1 catalysts. (a) XRD patterns; (b) XPS spectra; (c) H_2-TPR profiles and (d) NH_3-TPD results.

with 86.2 % HCN selectivity. In addition, the support effect of Cu catalysts has been investigated, as shown in Figure S7, Table S1 and Table S2, and S-1 exhibits the best performance. Furthermore, using S-1 as support, the effect of metal type has also been studied, as shown in Figure S8, and Cu shows the best performance.

The results of the ARM reaction at 673 K for 24 hours continuous operation are shown in Figure 2 b. Initially, we achieved 30 % CH_4 conversion and 79 % HCN selectivity. However, these values slightly decreased in the course of the experiment, probably due to carbon deposition, covering Cu active sites. After 24 hours continuous reaction, we still obtain 28 % CH_4 conversion and 71 % HCN selectivity, indicating a

good catalytic stability of the Cu/S-1 catalyst in CH_4/NH_3 NTP for the production of HCN and H_2.

As shown in Figure 3 a, the XRD patterns of S-1, fresh Cu/S-1 and spent Cu/S-1 samples clearly show five peaks at the lower diffraction angles, i.e., 7.9°, 8.8°, 23.1°, 24° and 24.4°, which are assigned to the MFI structure of the S-1 zeolite,[17] indicating that the lattice structure of S-1 was not damaged during either catalyst preparation or catalytic test. In addition, diffraction peaks of CuO (35.6° and 38.7°) and Cu (43.3°, 50.4° and 74.1°) can be identified in the XRD patterns of the fresh and spent Cu/S-1 samples, respectively, which means that CuO is reduced to metallic Cu during catalytic test.[18,19] The XPS spectra of fresh and spent Cu/S-1 samples are shown in Figure 3 b. For the fresh Cu/S-1 sample, the binding energies of Cu $2p_{3/2}$ and Cu $2p_{1/2}$ are found to be 933.8 eV (with a shake-up satellite at 943 eV) and 953.8 eV (with a shake-up satellite at 963 eV), respectively, which are assigned to Cu^{2+} species. For the spent Cu/S-1 sample, the binding energies of Cu $2p_{3/2}$ and Cu $2p_{1/2}$ decreased to 932.7 eV (without shake-up satellite) and 952.7 eV (without shake-up satellite), respectively, which are attributed to Cu^0 species.[20,21] Hence, the XPS results show the transformation of Cu^{2+} to Cu^0 species during the reaction, which is consistent with the results obtained by XRD (CuO to Cu), even when XPS is a surface sensitive technique, while XRD is a bulk technique.

The H_2-TPR profiles of the fresh and spent Cu/S-1 samples (Figure 3 c) indicate a significant peak (423-573 K) for the fresh Cu/S-1 catalyst, pointing towards the reduction of CuO to Cu,[22] while the spent Cu/S-1 sample exhibits no peaks of H_2 consumption, showing the metallic Cu phase. The H_2-TPR,

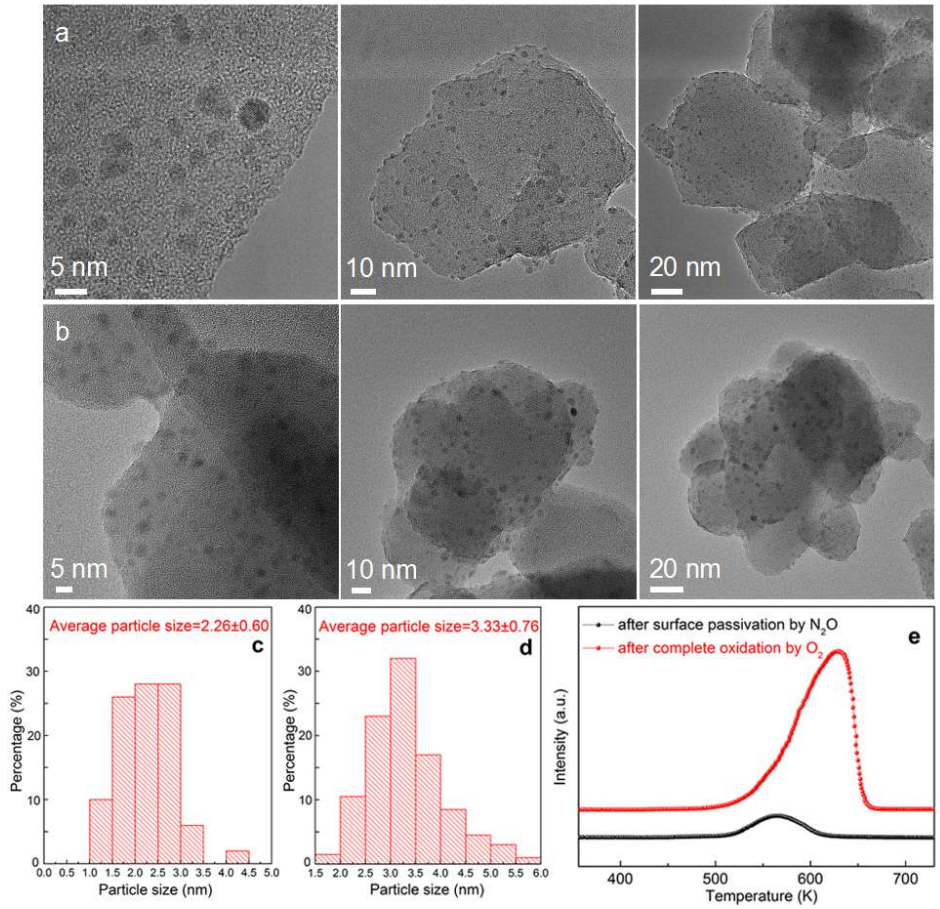

Figure 4. HRTEM patterns of (a) fresh Cu/S-1 catalyst and (b) spent Cu/S-1 catalyst, (c) CuO particle size distribution of fresh Cu/S-1 catalyst, (d) Cu particle size distribution of spent Cu/S-1 catalyst, and (e) H_2-TPR profiles of spent Cu/S-1 sample after surface passivation by N_2O and after complete oxidation by O_2 (result in e aims to titrate the number of surface Cu atom, so as to calculate the dispersity of Cu).

along with XRD and XPS, thus proves the transformation of CuO to metallic Cu phase during the ARM reaction process, implying that metallic Cu is the real active phase for the ARM reaction driven by plasma. The NH_3-TPD experiments were carried out to measure the acidity of S-1, fresh Cu/S-1 and spent Cu/S-1 samples (Figure 3 d). No desorption peaks are observed for the S-1 sample, indicating that NH_3 does not chemisorb onto the S-1 support, mainly because S-1 zeolite has no acid sites. However, desorption peaks of NH_3 are obvious for both fresh and spent Cu/S-1 samples, which means that NH_3 interacts strongly with both CuO and Cu, resulting in chemisorption of NH_3 on both fresh and spent Cu/S-1 catalysts.

Figure 4 show HRTEM images of fresh and spent Cu/S-1 sample. Clearly, Cu was highly dispersed on the S-1 support. The particle size distribution of CuO, derived from the HRTEM images with 5 nm and 10 nm scale, is plotted in Fig-

ure 4 c, and shows that the average size of the CuO particles is 2.1-2.2 nm. Figure 4 b shows HRTEM images of spent Cu/S-1 sample, and the particle size distribution of Cu is plotted in Figure 4 d. It can be seen that the average size of the Cu particles is 3.3 nm, which is bigger than that of the fresh CuO particles (2.1-2.2 nm), due to aggregation under the reaction conditions.

The dispersity of Cu (proportion of surface Cu atoms in the total Cu atoms) in the spent Cu/S-1 catalyst has been measured by N_2O chemisorption experiment (N_2O titration), as shown in Figure 4 e. The ratio of H_2 consumption after surface passivation by N_2O (reaction (3) and (4)) to H_2 consumption after complete oxidation by O_2 (reaction (5) and (6)) equals 0.1325, indicating a dispersity of 26.5% (equivalent to 3.77 nm of Cu particle size under the assumption of spherical particles, similar to that obtained by HRTEM). Based on the Cu dispersity (26.5 %) and Cu loading (10.1 % detected by XRF), as well as the reaction results (Figure 2), the turnover frequency (TOF) of HCN generation on Cu/S-1 catalyst is calculated to be 2.54 h^{-1}. As shown in Table S3, the TOF of Pt/TS-1 catalyst is 17.66 h^{-1}. However, the TOF of Cu increases with Cu loading, and it reaches 9.59 h^{-1} at 30 wt.% loading. As can be seen from Table S3, the dispersion of Cu dramatically decreases with increasing Cu loading. Note that the dispersion degree of Cu is achieved by N_2O titration experiments, which is the most definitive method for determining the dispersion of Cu. Hence, with increasing Cu loading, the effective number of active sites (surface Cu atoms) decreases, which is caused by a bigger particle size at higher loading. Furthermore, the catalyst granule sizes have no influence on reaction performance (Figure S9), which means that there is no internal diffusion limitation in this reaction. Thus, from the catalytic point of view, the lower the dispersion of Cu, the higher the TOF value, indicating that the plasma-catalytic CH_4/NH_3 reaction to produce HCN and H_2 is a structure-sensitive reaction.

$$2Cu\ (s) + N_2O \rightarrow Cu_2O\ (s) + N_2 \qquad (3)$$

$$Cu2O\ (s) + H_2 \rightarrow 2Cu\ (s) + H_2O \qquad (4)$$

$$2Cu + O_2 \rightarrow 2CuO \qquad (5)$$

$$CuO + H_2 \rightarrow Cu + H_2O \qquad (6)$$

To further demonstrate that the active sites for the ARM reaction are in the metallic Cu phase, we detected the species in the product gas in-situ by mass spectrometry (MS), as shown in Figure S10, for both the fresh and spent Cu/S-1 samples. When using fresh Cu/S-1 sample, no HCN was detected in the initial stage, but instead, we can clearly see water droplets on the inner wall of the exhaust pipe, attributed to the reduction of CuO to Cu by NH_3 (equation (7)). After the reduction process, the signal of HCN and H_2 dramatically increased and then remained stable (see Figure S7 a), indicative for the ARM reaction producing HCN and H_2. When using the spent Cu/S-1 sample, the signal of HCN and H_2 dramatically increased over the first 10 min, and then remained stable, implying that the ARM reaction can directly proceed on the spent Cu/S-1 catalysts to produce HCN and H_2. In other words, the catalytically active sites for the ARM reaction are in the metallic Cu phase.

$$3CuO + 2NH_3 \rightarrow 3Cu + 3H_2O + N_2 \qquad (7)$$

To understand the reaction mechanism of the plasma-catalytic ARM process, we performed in situ optical emission spectroscopy (OES) diagnostics of the CH_4/NH_3 plasma, aiming to identify the reactive species. As shown in Figure 5 a, when using plasma without catalyst, we collected three main molecular spectral bands at 564-567 nm, 610-670 nm and 720-780 nm. The first band at 564-567 nm belongs to deexcitation of electronically excited NH_3* (Schuster band),[23] while the latter two bands are attributed to deexcitation of electronically excited NH_2* radicals (alpha band).[24] A partial enlargement of the OES profile for the 320-440 nm range (inset in Figure 5 a) shows the emission line at 336 nm, which is assigned to the deexcitation of electronically excited NH* radicals ($A^3\prod \rightarrow X^3S^-$).[25] These ammonia-related OES signals demonstrate the presence of NH_2 and NH species in the CH_4/NH_3 plasma. In addition, the line at 431 nm is assigned to the decay of CH* radicals ($A^2\sum \rightarrow X^2\prod$),[26] demonstrating the presence of CH radicals as well. Generally, in NTP, CH* radicals are produced through cascade dehydrogenation of CH_4, i.e., $CH_4 \rightarrow CH_3 \rightarrow CH_2 \rightarrow CH$, and the probabilities of generating CH_3, CH_2 and CH radicals have been modeled to be 79 %, 15 % and 5 %, respectively.[27] Although the exact composition will depend on the conditions, we should also expect more CH_3 and CH_2 than CH radicals in our case. Therefore, the OES signal of CH* (431 nm) also indicates the existence of CH_3 and CH_2 radicals in the CH_4/NH_3 plasma. The reason why CH_3 and CH_2 were not detected by OES is because their emission lines appear in the infrared region, which is out of the wavelength range of our OES measurements. Finally, the line at 388 nm corresponds to the decay of CN*, i.e., $B^2\sum \rightarrow X^2\sum$,[28] which indicates the presence of CN radicals in the plasma, produced by the reaction between CH_x and NH_x radicals. In summary, CH_x (CH_3, CH_2 and CH), NH_x (NH_2 and NH) and CN radicals are present in our CH_4/NH_3 plasma without catalyst.

As shown in Figure 5 b, when the CH_4/NH_3 plasma was packed by S-1 zeolite (plasma + S-1), the OES intensities reduced a lot, which is caused by optical shielding due to the granules. Interestingly, when packing with Cu/S-1 catalyst, the OES bands and lines nearly disappeared, implying that the excited species are adsorbed by the metallic Cu active sites.

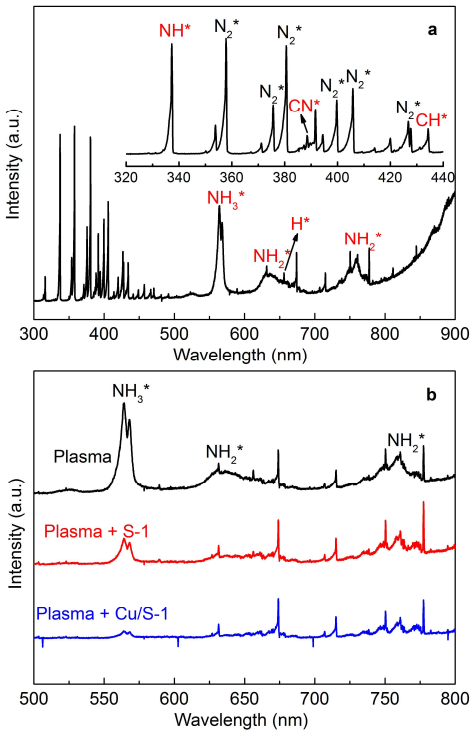

Figure 5. Optical emission spectra of CH_4/NH_3 DBD plasma at 673 K, (a) without catalyst, and (b) comparison between plasma-only, plasma + S-1, and plasma + Cu/S-1 catalyst.

In order to understand how the plasma-induced radicals detected by OES contribute to the plasma-catalytic conversion process, and thus to understand why the catalytic process is activated by the plasma, we performed dispersion-corrected density functional theory (DFT) calculations to find the minimum energy path (MEP) for the reactions of N, NH, CH and NH_2 to produce HCN on various Cu surfaces. Based on the surface morphology seen in the XRD patterns (Figure 3 a), we employed Cu (111), Cu (200) and Cu (220) slabs for the calculations. In contrast to thermal catalysis, where the reactions normally occur via the Langmuir-Hinshelwood (LH) mechanism,[29] in plasma catalysis both Eley-Rideal (ER) and LH mechanisms can occur,[30] and depending on the mechanism to proceed, the reaction barrier will be different. In Figure 6, we summarize the elementary steps of C-N coupling, as well as the formation of hydrogenated intermediates and their dehydrogenation to HCN, considered in our calculations, occurring through both ER and LH mechanisms.

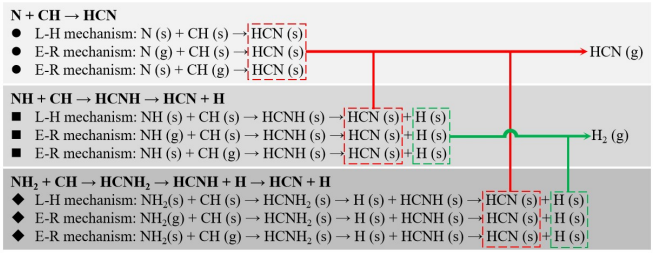

Figure 6. Elementary steps of C-N coupling, formation of hydrogenated intermediates and their dehydrogenation to HCN through ER and LH mechanisms, considered in our calculations.

The activation energies calculated for these reactions are listed in Table 1. The values in parentheses represent the reaction barriers for these endothermic reactions, in which no saddle point is detected along the path. The equilibrium bond lengths calculated for HCN in gas phase (C-N: 1.158 Å and C-H: 1.074 Å) are in good agreement with experimental and theoretical data.[31,32]

Table 1. Calculated activation energy of the elementary steps of C-N coupling, formation of hydrogenated intermediates and their dehydrogenation to HCN through ER and LH mechanisms, as well as for the desorption of HCN and H_2, on Cu (111), (200) and (220) crystal planes. The values in parentheses are reaction energies instead of activation energies. All values are in eV.

No.	Reaction	Cu (111)	Cu (200)	Cu (220)
8	N (s) + CH (s)→ HCN (s)	0.78	0.75	0.62
9	N (g) + CH (s)→ HCN (s)	0.00	0.00	0.00
10	N (s) + CH (g)→ HCN (s)	0.00	0.00	0.00
11	HCN (s) → HCN (g)	(0.83)	(0.70)	(0.88)
12	NH (s) + CH (s) → HCNH (s)	0.45	0.50	0.72
13	NH (g) + CH (s) → HCNH (s)	0.00	0.00	0.00
14	NH (s) + CH (g) → HCNH (s)	0.00	0.00	0.00
15	HCNH (s) → HCN (s) + H (s)	1.38	1.32	1.48
16	NH_2 (s) + CH (s) → $HCNH_2$ (s)	1.20	1.60	1.54
17	NH_2 (g) + CH (s) → $HCNH_2$ (s)	0.00	0.00	0.00
18	NH_2 (s) + CH (g) → $HCNH_2$ (s)	0.00	0.00	0.00
19	$HCNH_2$ (s) → HCNH (s) + H (s)	1.27	1.25	1.30
20	H (s) + H (s) → H_2 (g)	1.01	0.91	0.89

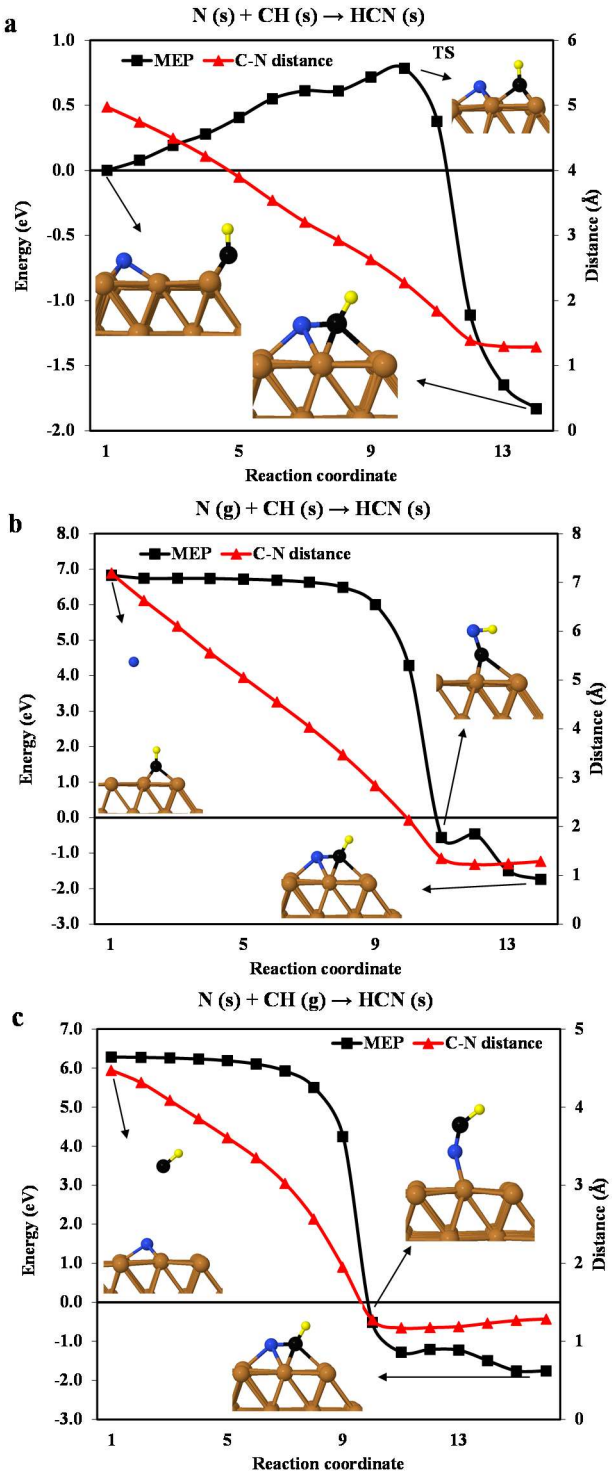

Figure 7. Minimum energy path (MEP; black curve, left y-axis) and C-N distance (red curve, right y-axis) for (a) the interaction of pre-adsorbed N and CH, (b) gas phase N with pre-adsorbed CH and (c) gas phase CH with pre-adsorbed N to form HCN(s) on the Cu (111) surface. All energies are with respect to that of the pre-adsorbed N and CH on Cu (111). The insets illustrate the configurations of initial state, transition state (TS) and final state, where brown, black, blue and yellow colors correspond to Cu, C, N and H atoms, respectively.

For direct C-N coupling as one of the most critical steps in HCN synthesis, we can see that the reactions happening via the ER mechanism are barrierless, thanks to the high reactivity of the plasma radicals. For instance, Figures 7 shows the interaction of N and CH to form HCN via both LH and ER mechanisms (reactions 8, 9 and 10) on the Cu (111) surface (corresponding to the highest intensity in the XRD patterns of Figure 3 a). The LH interaction of pre-adsorbed N(s) and CH(s) (reaction 8) exhibits a reaction barrier of 0.78 eV towards the formation of HCN (Figure 7 a).

Figure 7 b and c show the same reaction via both ER mechanisms (reaction 9 and 10). In this case the energy of the initial gas phase radicals is much higher, so the whole configuration is highly unstable, representing the non-equilibrium status of the plasma-catalytic system. As displayed in Figure 7 b, N is initially in gas phase and approaches the pre-adsorbed CH(s). At the C-N distance around 3.47 Å, N(g) enters the reaction channel and the energy of the system decreases steeply. The same happens to the alternative ER pathway, starting with gas phase CH interacting directly with pre-adsorbed N(s) (Figure 7 c). CH(g) experiences the van der Waals attraction at a C-N distance around 3.02 Å and the gas phase radical falls into the lower energy levels towards coupling with N. We observed the same pattern for all the reactions occurring through the ER mechanism, and on all three Cu surfaces, which emphasizes that the C-N coupling reactions containing gas phase radicals can easily happen via this mechanism, without the need to overcome any reaction barrier (see Figures S11 and S12).

These results are consistent with our OES spectra, showing the disappearance of the excited species with the Cu/S-1 catalyst packing (Figure 5). The highly reactive N, NH, NH_2 and CH radicals created in the plasma either interact directly with pre-adsorbed species or get adsorbed on the Cu surface, to be involved in LH reactions. The barrierless C-N coupling via the ER mechanism can explain why HCN formation can proceed in plasma catalysis at 673 K, with high conversion, while this is not possible in thermal catalysis at such low temperature, due to the relatively large activation barriers for CH4 dissociation and C-N bond formation, as the most critical steps in HCN synthesis.

For the dehydrogenation step of the hydrogenated intermediates, i.e., HCNH and $HCNH_2$, Table 1 suggests that the activation barriers for the reactions taking place on the rougher Cu (220) are slightly higher than for the same reactions occurring on the flatter Cu (111) and Cu (200) surfaces. This suggests that the dehydrogenation steps are more likely to happen on Cu (111) and Cu (200) surfaces. However, a more detailed study considering the highly complex network of possible reaction pathways and coverage effects is needed to determine the surface sensitivity of the plasma-assisted HCN synthesis from ammonia and methane.

Conclusion

In conclusion, we demonstrated plasma-catalytic ammonia reforming of methane (ARM) at 673 K for the production of HCN and H_2 using CH_4/NH_3 plasma with Cu/S-1 catalyst, reaching 30 % CH_4 conversion with 79 % HCN selectivity and stoichiometric H_2. Catalyst characterization results clearly

illustrate that highly dispersed metallic Cu particles (2-3 nm) are the catalytically active centers in plasma-catalytic ARM. By combined experimental and DFT calculation results, we can conclude that HCN production in plasma catalysis is mainly attributed to the barrierless ER reactions between radicals generated in plasma and adsorbed species over the Cu surface, as shown in Scheme 1. Note that the obtained energy consumption may not yet be the best achievable number. It may be possible to further optimize the plasma-driven process, to close the gap of energy consumption by optimizing reaction conditions (flow rate, residence time, etc.), catalysts (local environment of Cu particles, etc.) and plasma state (spark discharge, arc discharge, pulse discharge, etc.).

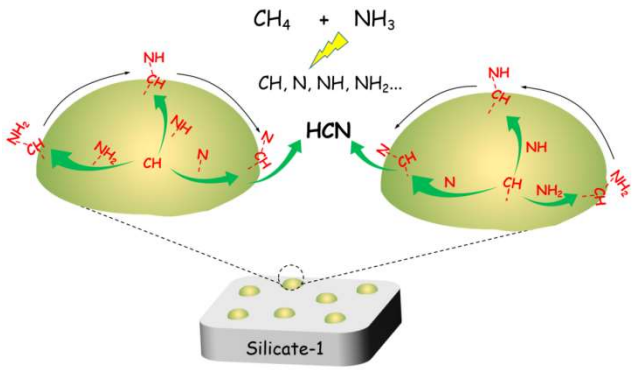

Scheme 1. Schematic diagram of the reaction mechanism in plasma-catalytic ARM for HCN synthesis. (left) reaction between pre-adsorbed CH and gas phase NH_x; (right) reaction between gas phase CH and pre-adsorbed NH.

ASSOCIATED CONTENT

Supporting Information.

The Supporting information is available free of charge on the Internet at http://pubs.acs.org.

More experiment details, characterizations, and catalytic results.

AUTHOR INFORMATION

Corresponding Author

* E-mail: yiyanhui@dlut.edu.cn

Notes

The authors declare no competing financial interest.

ACKNOWLEDGMENT

We acknowledge financial support from the National Natural Science Foundation of China [21503032], the China Postdoctoral Science Foundation [grant numbers 2015M580220 and 2016T90217, 2016], PetroChina Innovation Foundation [2018D-5007-0501] and the TOP research project of the Research Fund of the University of Antwerp [grant ID 32249].

REFERENCES

(1) Ertl, G.; Knözinger, H.; Schüth, F.; Weitkamp, J. Handbook of Heterogeneous Catalysis, 2nd ed.; Wiley-VCH, John Wiley: Weinheim, 2008; Vol. 8, p 2593.

(2) Sherwood, T. K.; Gilliland, E. R.; Ing, S. W. Hydrogen cyanide synthesis from elements and from ammonia and carbon. *Ind. Eng. Chem.* **1960**, *52*, 601-604.

(3) Grabow, L. C.; Studt, F.; Abild-Pedersen, F.; Petzold, V.; Kleis, J.; Bligaard, T.; Nørskov, J. K. Descriptor-based analysis applied to HCN synthesis from NH_3 and CH_4. *Angew. Chem. Int. Ed.* **2011**, *50*, 4601-4605.

(4) Johnson, G. E.; Decker, W. A.; Forney, A. J.; Field, J. H. Hydrogen cyanide produced from coal and ammonia. *Ind. Eng. Chem. Process Des. Dev.* **1968**, *7*, 137-143.

(5) Koszinowski, K.; Schröder, D.; Schwarz, H. Probing cooperative effects in bimetallic clusters: Indications of C-N coupling of CH_4 and NH_3 mediated by the cluster ion $PtAu^+$ in the gas phase. *J. Am. Chem. Soc.* **2003**, *125*, 3676-3677.

(6) Bodke, A. S.; Olschki, D. A.; Schmidt, L. D. Hydrogen addition to the Andrussow process for HCN synthesis. *Appl. Catal. A* **2000**, *201*, 13-22.

(7) Kondratenko, V. A. Mechanistic analysis of oxygen-assisted coupling of methane and ammonia to hydrogen cyanide over polycrystalline Pt and Rh. *Catal. Sci. Technol.* **2015**, *5*, 1598-1605.

(8) Aschi, M.; Brönstrup, M.; Diefenbach, M.; Harvey, J. N.; Schröder, D.; Schwarz, H. A gas-phase model for the Pt^+-catalyzed coupling of methane and ammonia. *Angew. Chem. Int. Ed.* **1998**, *37*, 829-832.

(9) Zhou, S.; Li, J.; Schlangen, M.; Schwarz, H. Bond activation by metal-carbene complexes in the gas phase. *Accounts Chem. Res.* **2016**, *49*, 494-502.

(10) Herceg, E.; Trenary, M. Formation of surface CN from the coupling of C and N atoms on Pt(111). *J. Am. Chem. Soc.* **2003**, *125*, 15758-15759.

(11) Diefenbach, M.; Brönstrup, M.; Aschi, M.; Schröder, D.; Schwarz, H. HCN synthesis from methane and ammonia: mechanisms of Pt^+-mediated C-N coupling. *J. Am. Chem. Soc.* **1999**, *121*, 10614-10625.

(12) Xu, S.; Chansai, S.; Stere, C.; Inceesungvorn, B.; Goguet, A.; Wangkawong, K.; Taylor, S. F. R.; Al-Janabi, N.; Hardacre, C.; Martin, P. A.; Fan, X. Sustaining metal-organic frameworks for water-gas shift catalysis by non-thermal plasma. *Nat. Catal.* **2019**, *2*, 142-148.

(13) Snoeckx, R.; Bogaerts, A. Plasma technology-a novel solution for CO_2 conversion?. *Chem. Soc. Rev.* **2017**, *46*, 5805-5863.

(14) Mehta, P.; Barboun, P.; Herrera, F. A.; Kim, J.; Rumbach, P.; Go, D. B.; Hicks, J. C.; Schneider, W. F. Overcoming ammonia synthesis scaling relations with plasma-enabled catalysis. *Nat. Catal.* **2018**, *1*, 269-275.

(15) Guo, Z.; Yi, Y.; Wang, L.; Yan, J.; Guo, H. Pt/TS-1 catalyst promoted C-N coupling reaction in CH_4-NH_3 plasma for HCN synthesis at low temperature. *ACS Catal.* **2018**, *8*, 10219-10224.

(16) Gail, E.; Gos, S.; Kulzer, R.; Lörsch, J; Sauer, M. Ullmann's Encyclopedia of Industrial Chemistry, Wiley-VCH: Weinheim, 2012; Vol. 10, p 677.

(17) Zhu, H.; Liu, Z.; Wang, Y.; Kong, D.; Yuan, X.; Xie, Z. Nanosized $CaCO_3$ as hard template for creation of intracrystal pores within silicalite-1 crystal. *Chem. Mater.* **2008**, *20*, 1134-1139.

(18) Gong, J.; Yue, H.; Zhao, Y.; Zhao, S.; Zhao, L.; Jing, L.; Wang, S.; Ma, X. Synthesis of ethanol via syngas on Cu/SiO_2 catalysts with balanced Cu^0-Cu^+ sites. *J. Am. Chem. Soc.* **2012**, *134*, 13922-13925.

(19) Lomate, S.; Sultana, A.; Fujitani, T. Effect of SiO_2 support properties on the performance of Cu-SiO_2 catalysts for the hydrogenation of levulinic acid to gamma valerolactone using formic acid as a hydrogen source. *Catal. Sci. Technol.* **2017**, *7*, 3073-3083.

(20) Biesinger, M. C.; Lau, L. W. M.; Gerson, A. R.; Smart, R. S. C. Resolving surface chemical states in XPS analysis of first row transition metals, oxides and hydroxides: Sc, Ti, V, Cu and Zn. *Appl. Surf. Sci.* **2010**, *257*, 887-898.

(21) Natesakhawat, S.; Lekse, J. W.; Baltrus, J. P.; Ohodnicki, P. R.; Howard, B. H.; Deng, X.; Matranga, C. Active sites and structure-activity relationships of copper-based catalysts for carbon dioxide hydrogenation to methanol. *ACS Catal.* **2012**, *2*, 1667-1676.

(22) Ciocîlteu, S. M.; Salou, M.; Kiyozumi, Y.; Niwa, S.; Mizukami, F.; Haneda, M. Uniform distribution of copper and cobalt during the synthesis of SiMFI-5 from kanemite through solid-state transformation. *J. Mater. Chem.* **2003**, *13*, 602-607.

(23) Yi, Y.; Zhang, R.; Wang, L.; Yan, J.; Zhang, J.; Guo, H. Plasma-triggered CH_4/NH_3 coupling reaction for direct synthesis of liquid nitrogen-containing organic chemicals. *ACS Omega* **2017**, *2*, 9199-9210.

(24) Herzberg, G.; Ramsay, D. A. Absorption spectrum of free NH_2 radicals. *J. Chem. Phys.* **1952**, *20*, 347-347.

(25) Yasui, K.; Arayama, T.; Okutani, S.; Akahane, T. Generation of ammonia plasma using a helical antenna and nitridation of GaAs surface. *Appl. Surf. Sci.* **2003**, *212*, 619-624.

(26) Tu, X.; Whitehead, J. C. Plasma-catalytic dry reforming of methane in an atmospheric dielectric barrier discharge: Understanding the synergistic effect at low temperature. *Appl. Catal. B* **2012**, *125*, 439-448.

(27) Wang, L.; Yi, Y.; Wu, C.; Guo, H.; Tu, X. One-step reforming of CO_2 and CH_4 into high-value liquid chemicals and fuels at room temperature by plasma-driven catalysis. *Angew. Chem. Int. Ed.* **2017**, *56*, 13679-13683.

(28) Langereis, E.; Knoops, H. C. M.; Mackus, A. J. M.; Roozeboom, F.; van de Sanden, M. C. M.; Kessels, W. M. M. Synthesis and in situ characterization of low-resistivity TaN_x films by remote plasma atomic layer deposition. *J. Appl. Phys.* **2007**, *102*, 083517.

(29) Ertl, G. Reactions at surfaces: From atoms to complexity (Nobel lecture). *Angew. Chem. Int. Ed.* **2008**, *47*, 3524-3535.

(30) Shirazi, M.; Neyts, E. C.; Bogaerts, A. DFT study of Ni-catalyzed plasma dry reforming of methane. *Appl. Catal. B* **2017**, *205*, 605-614.

(31) WOODS, R. C. Microwave spectroscopy of molecular ions in the laboratory and in space. *Philos. Trans. R. Soc. A-Math. Phys. Eng. Sci.* **1988**, *324*, 141-146.

(32) Xu, L. T.; Dunning, T. H. Variations in the nature of triple bonds: The N_2 , HCN, and HC_2H series. *J. Phys. Chem. A.* **2016**, *120*, 4526-453.